Study of rotational dynamics of receptor-targeted contrast agents in cancerous and normal prostate tissues using time-resolved picosecond emission spectroscopy

Yang Pu,[1] Wubao B. Wang,[1] Samuel Achilefu,[2] and R. R. Alfano[1,*]

[1]Institute for Ultrafast Spectroscopy and Lasers, The City College of the City University of New York, Convent Avenue at 138th Street, New York, New York 10031, USA

[2]Washington University School of Medicine, 4525 Scott Avenue, St. Louis, Missouri 63110, USA

*Corresponding author: alfano@sci.ccny.cuny.edu

Received 28 June 2010; revised 12 January 2011; accepted 6 January 2011; posted 27 January 2011 (Doc. ID 130675); published 24 March 2011

We studied the time-resolved polarization-dependent fluorescence spectroscopy of receptor-targeted contrast agents (Cybesin and Cytate) bound with prostate cancer cells in prostate tissue. An analytical model dealing with highly viscous tissue media was developed and used to investigate the rotation times and fluorescence anisotropies of the receptor-targeted contrast agents in prostate tissue. The differences of rotation times and fluorescence anisotropies were observed for Cybesin (Cytate) in cancerous and normal prostate tissues, which reflect changes of the microstructures of cancerous and normal tissues and their different bound affinity with contrast agents. The preferential uptake of Cytate (Cybesin) in cancerous tissue was used to image and distinguish cancerous tissue areas from normal tissue areas. The fluorescence polarization difference imaging technique was used to enhance the image contrast between the cancerous and normal tissue areas. This research may help to introduce a new optical approach and criteria for prostate cancer detection.

OCIS codes: 170.6510, 170.6930, 170.3880, 300.6500.

1. Introduction

Prostate cancer has a high incidence and mortality rate for men. In 2009, new cases of prostate cancer were diagnosed nearly 192,280 times, ranking as No. 1 of new cancer incidence for men in the U.S. [1]. Inspired by the initial research of Alfano's group in the 1980s [2], fluorescence spectroscopy has been widely studied as an optical tool for cancer diagnosis. Time-resolved fluorescence polarization spectroscopy measures the temporal intensity profile and degree of emission polarization within its lifetime, and it provides information not only of the location of abnormalities but also their biophysical microenvironments [3,4]. The use of intrinsic chromophores to differentiate optical properties of diseased and healthy human tissues is limited by their ultraviolet bands [5], which are not in the near-infrared (NIR) range of "tissue optical window" [6].

Recent progress in biomedicine has shown that attachment of the optical dyes emitting desirable wavelengths to small molecular peptides (ligand) can be used to target overexpressed receptors on certain tumors without loss of receptor affinity of the ligand [7]. Two kinds of receptor-targeted contrast agents, namely Cybesin and Cytate, were demonstrated to target the overexpressed bombesin receptor (BR) [8] and somatostatin receptor (SSTR) [9], respectively, on prostate cancer tissues *in vitro* [10,11]. The advantages of optical receptor-targeted contrast agents include a high affinity of specific

0003-6935/11/101312-11$15.00/0

ligand corresponding to overexpressed receptor for the localization of tumors [7], rapid clearance of the applied contrast, possibilities of preparing a library of peptides for rapid identification of bioactive molecules [7], and preservation of spectral advantage in the NIR range of the "tissue optical window" [10,11]. Time-resolved polarization-dependent fluorescence spectroscopy provides not only the intensity information but also relaxation and rotation information of fluorophores in the microenvironment of media [3]. Gleason grades for prostate cancer stages indicate that there are different microstructures of cancerous prostate tissue in comparison with normal prostate tissue: high cell density, nonuniform cell distribution, and enlarged nuclei size in cancerous tissue [12].

In this study, an analytical model was developed and used to describe the time-resolved polarized fluorescence kinetics of the contrast agents (Cybesin and Cytate) in prostate tissue. The rotation times and fluorescence anisotropies of the receptor-targeted contrast agents in stained cancerous and normal prostate tissues were extracted using this analytical model with the measured time-resolved polarized fluorescence data. The differences of rotation times and fluorescence anisotropies were observed for Cybesin (Cytate) in cancerous and normal prostate tissues. These differences reflect changes of microstructures of cancerous and normal tissues, and a much larger portion of contrast agents conjugated with the cancerous cells than that with the normal.

2. Experimental Samples and Method

The experimental arrangement of the time-resolved fluorescence measurements has been reported elsewhere [3]. Ultrafast 130 fs laser pulses at 800 nm were generated with a repetition rate of 82 MHz from a mode-locked Ti:sapphire laser system and used to pump the samples (Cybesin- and Cytate-stained cancerous or normal prostate tissues). The fluorescence was collected by a lens with 5 cm focus length into a synchroscan streak camera with a temporal resolution of 10 ps. An 830 nm long pass filter was used to cut off the illuminating light so that only the emission from the sample was recorded. Two polarizers (P_1 and P_2) were used. P_1 was used to ensure the linear polarization of the input laser pulses and P_2 used as an analyzer. The polarization of P_2 was rotated from 0° to 90° with respect to that of P_1 to record the intensity profiles of the parallel and perpendicular polarization components of the fluorescence. The temporal profiles recorded by a silicon-intensified target of the streak camera were analyzed to obtain temporal and polarization information of the fluorescence.

Cybesin (Cytate) was synthesized by Achilefu's group at the Washington University School of Medicine. Cybesin (Cytate) is mainly composed of ICG (an FDA-approved NIR dye) and the BR (SSTR) ligand, which delivers ICG to the corresponding receptors overexpressed in tumor [7]. Human prostate tissues were obtained from the Co-operation Human Tissue Network (CHTN) and the National Disease Research Interchange (NDRI) under the approval of the Institutional Review Board at The City College of the City University of New York. Each pair of cancerous and normal prostate tissue samples was taken from the same patient, and diagnosed by a pathology medical doctor. Samples were neither chemically treated nor were frozen prior to the experiments. The time elapsed between tissue resection and measurements may vary for different sample sources. However, the maximum elapsed time is less than 30 h. The preparation of prostate tissue samples used for time-resolved studies follows this protocol: (1) samples (cancerous and normal prostate tissues) were cut into $\sim 2 \times \sim 1 \times \sim 0.5$ cm (length × width × thickness) pieces, (2) samples were soaked in the same aqueous Cybesin (Cytate) with a concentration of $\sim 3.2 \times 10^{-6}$ M for ~10 min, (3) samples were put into sodium phosphate buffer (Sigma-Aldrich) to wash off and consequently reduce the amount of unbound Cybesin (Cytate) in particular on the surface and subsurface. Six pairs of samples were investigated for Cybesin targeting to overexpressed BR [7,8,10] in cancerous tissue and six for Cytate to SSTR [7,9,11]. For each prostate tissue sample, three to six different locations were measured to get an average value.

The spectral polarization imaging set up used for imaging Cybesin- and Cytate-stained cancerous and normal prostate tissues has been described in our early work [10]. Light from a white light source is used to illuminate the prostate tissue sample with average power of $\sim 50\,\mu W/cm^2$. The wavelengths of the pump and detection are selected using wide-band pass filters varying from 550 to 900 nm with FWHM = 40 nm. A CCD camera records images formed by light emitted from the sample. Polarizers were used to obtain parallel and perpendicular images relative to the polarization direction of the illuminating light.

A typical cancerous/normal prostate tissue sample used for the imaging measurements consists of a small piece of cancerous prostate tissue and a small piece of normal prostate tissue. They were first soaked in the same aqueous Cybesin (Cytate) with a concentration of $\sim 3.2 \times 10^{-6}$ M for ~10 min and then put into sodium phosphate buffer (Sigma-Aldrich) to wash off the unbound Cybesin (Cytate). The stained cancerous and normal tissues were then covered by a large piece of ~0.5 mm thick normal prostate tissue.

3. Analytical Model

A. Picosecond Rotational Diffusion Kinetic and Time-Resolved Fluorescence of Dyes in Solution

Picosecond rotational kinetic fluorescence spectroscopy is widely used to investigate the rotational motion of fluorophores in solution [13,14]. The

time-resolved polarization measurements of fluorophores excited with linearly polarized light can be applied as a probe to determine the rotation rate of dye molecules, which is a function of the viscosity and temperature of the environment, and the size of rotating molecule [13]. The ultrafast rotation dynamics of fluorophores can be used to extract the information of the surrounding medium [3]. The fluorescence depolarization property is usually described by the time-resolved fluorescence anisotropy, defined as [13,14]:

$$r(t) = \frac{I_{\parallel}(t) - I_{\perp}(t)}{I_{\parallel}(t) + 2I_{\perp}(t)}, \tag{1}$$

where $I_{\parallel}(t)$ and $I_{\perp}(t)$ are the emission intensities of the fluorescent components whose polarizations are parallel and perpendicular to the polarization direction of the excited light, respectively [13,14]. Equation (1) shows the relationships between the time evolution of $r(t)$ and the measured intensities of the fluorescence components, $I_{\parallel}(t)$ and $I_{\perp}(t)$. The depolarization feature of emission from contrast agents in solvent is realized to be mainly caused by Brownian rotation [13–15]. Therefore, it is possible to determine the rotation rate of molecules from measured $I_{\parallel}(t)$ and $I_{\perp}(t)$. The picosecond polarized fluorescence of a dipole can be described by a set of equations containing two parameters: the decay rate of the emission of their excited state (reflecting the dipole's lifetime) and the transport rate of the emission from one orthogonal component to another (reflecting the dipole's rotation time) [9]. The decay of the parallel $[I_{\parallel}(t)]$ and perpendicular $[I_{\perp}(t)]$ components of the fluorescence excited by a linear polarized light beam can be described by [15]:

$$\begin{aligned} I_{||}(t) &= \frac{I_0}{3}\exp\left(-\frac{t}{\tau_f}\right)\left(1 + 2r_0\exp\left(-\frac{t}{\tau_r}\right)\right), \\ I_{\perp}(t) &= \frac{I_0}{3}\exp\left(-\frac{t}{\tau_f}\right)\left(1 - r_0\exp\left(-\frac{t}{\tau_r}\right)\right), \end{aligned} \tag{2}$$

where I_0 is the initial emission intensity, τ_f is the fluorophore's lifetime, τ_r is the rotation time affecting the depolarization rate of the emission of the excited polarized molecules, and r_0 is the initial fluorescence anisotropy at $t = 0$ reflecting the initial orientation of the dipoles. Substituting Eq. (2) into (1), $r(t)$ can be written as [13]:

$$r(t) = r_0\exp\left(-\frac{t}{\tau_r}\right). \tag{3}$$

Equation (3) indicates that the decay behavior of $r(t)$ is noted to reflect the dipole's rotation time (τ_r) but independent of the fluorescence lifetime (τ_f) of the molecules [13]. Theoretical calculation of r_0 is based on the physical phenomenon of photoselection: the population of excited fluorophores partially oriented along the parallel direction. The theoretical value of r_0 was calculated and reported to be 0.4 in solution [13–15]. In the simple possible case where molecules undergo Brownian rotation as Einstein spheres, the rotation time is determined as an Einstein–Stokes relationship [13]:

$$\tau_r = \frac{\eta V}{KT}, \tag{4}$$

where K is the Boltzmann constant, T is the absolute temperature, η is the viscosity of solvent, and V is the volume of a molecule.

The total fluorescence intensity $I(t)$ can be written as:

$$I(t) = I_{\parallel}(t) + 2I_{\perp}(t) = I_0\exp\left(-\frac{t}{\tau_f}\right), \tag{5}$$

where the factor of 2 is used for counting the contribution of the two perpendicular components to the whole fluorescence intensity because the dipoles' Brownian motion happens in 3D space. Equation (5) indicates that the temporal profiles of the total emission intensity $I(t)$ depends only on I_0 (the initial emission intensity) and τ_f (the fluorophore's lifetime) but not on τ_r (the dipole's rotation time).

B. Analytical Model: Static and Time-Resolved Components of Fluorescence Anisotropy of Receptor-Targeted Contrast Agents in Prostate Tissues

In order to investigate the time evolution of emission from receptor-targeted contrast agents (Cybesin and Cytate) bound with prostate cancer cells [7,10,11] in prostate tissue, an analytical model dealing with high viscous media was developed. It is well known that the properties of biological living tissues are somehow similar to the behavior of liquid with very high viscosity [16,17], and the human body has a volume of 70% to 80% water. Experimental results also indicated that dye in highly viscous tissues is expected to have an ordered structure to cause the different distribution of the initially excited fluorescent molecules while the time-resolved fluorescence polarization spectroscopy is measured [18]. The viscosities of prostate tissue were reported to be much higher than 3000 P [19]. Cybesin (Cytate) in prostate tissue can be considered as a fluorescent contrast agent in "highly viscous liquid."

After cancerous prostate tissue was soaked into the Cybesin (Cytate) solution and washed off using sodium phosphate buffer consequently, a large proportion of Cybesin (Cytate) was conjugated to the corresponding receptor on cells [7,10,11]. Although a large amount of free Cybesin (Cytate) molecules in surface and subsurface were removed by the buffer, some free contrast agents were still conserved in the deep tissue area. For the case of normal prostate tissue, a smaller portion of contrast agent was conjugated to tissue cells in comparison with cancerous tissue [7,10,11], and some free fluorescent molecules exist in the interstitial fluid of deep tissue areas. The

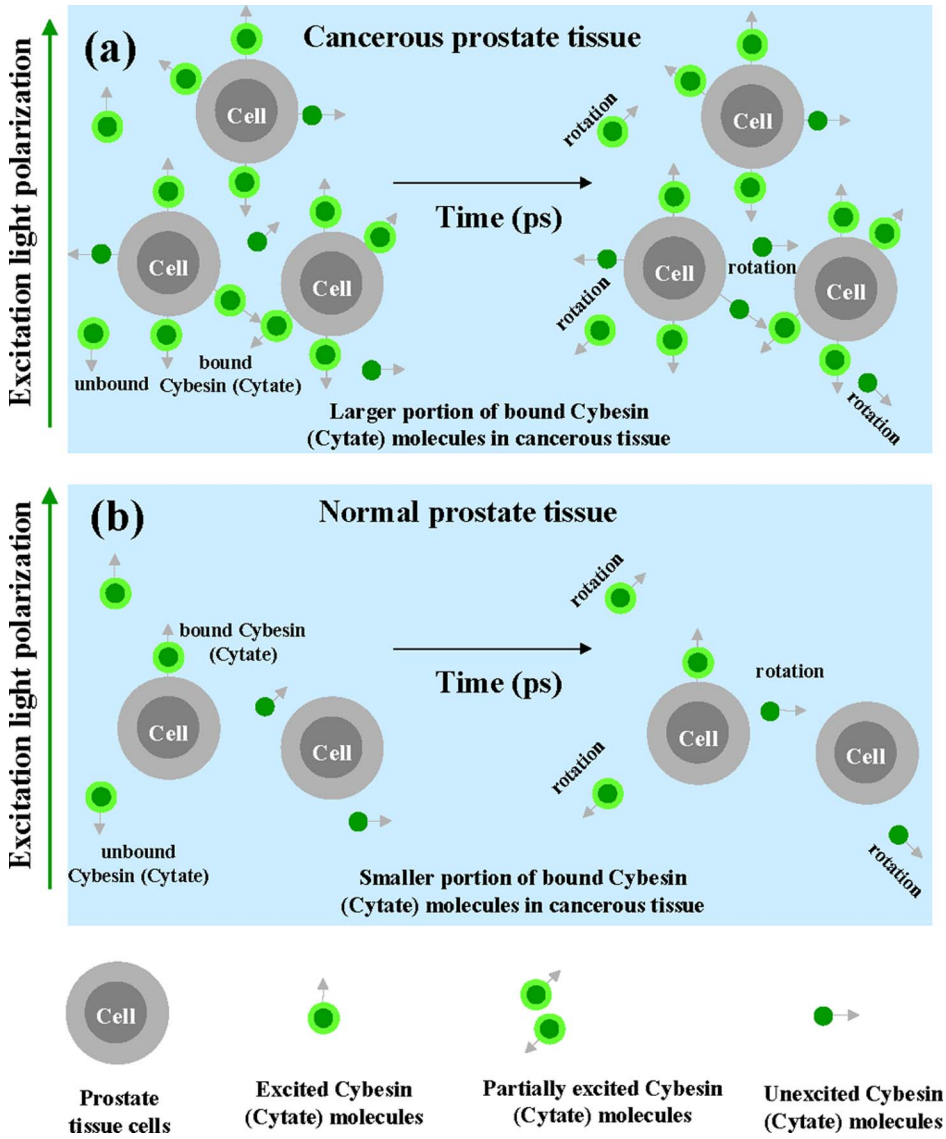

Fig. 1. (Color online) Schematic diagrams of the cell-bound mechanism and reorientation of Cybesin (Cytate) molecules in stained (a) cancerous tissue, which has a higher cell density and more cell-bound Cybesin (Cytate) molecules, and (b) normal tissue, which has a lower cell density and less cell-bound Cybesin (Cytate). Molecules with their absorption transition vectors (arrows) aligned parallel to the linearly polarized pump light (for example: vertical) and those having a parallel component of other-orientated transition vectors are excited. For free (unbound) molecules, the rapid rotations contribute to the fluorescence depolarization. In contrast, Cybesin (Cytate) molecules conjugated to prostate cells contribute to the static fluorescence anisotropy component.

cell-bound mechanism and reorientation of Cybesin (Cytate) molecules in prostate tissue is schematically shown in Fig. 1. This model describes two types of bound and unbound situations of Cybesin (Cytate) molecules in Cybesin (Cytate)-stained prostate tissues and their contributions to total fluorescence and fluorescence anisotropy.

As shown in Fig. 1, the emission of Cybesin (Cytate) can be considered to be contributed from two components: (i) static component caused by cell-bound Cybesin (Cytate) molecules in the prostate tissue and (ii) the temporal component contributed by the unbound Cybesin (Cytate) molecules that remain in the body liquid of prostate tissue and can undergo rotation. These assumptions are reasonable, because the weights of tissue cells are much larger than that of Cybesin (Cytate) molecules, and tissue cells are too huge to undergo rapid rotation. There are more cell-bound Cybesin (Cytate) molecules in cancerous prostate tissue than those in normal tissue, as indicated in Fig. 1, because of the overexpressed receptors on the prostate cancer cells and the highly bound affinity of the contrast agents to the corresponding receptors [11–15]. The free contrast agent molecules would undergo rotation, while the Cybesin (Cytate) molecules conjugated to the tissue cell would stay steady.

We consider a system of n types of noninteracting fluorophores and investigate the rotational dynamics and fluorescence anisotropies of the contrast agents

in prostate tissue. The total time-resolved fluorescence intensity of n types of noninteracting fluorophores is given by [20]:

$$I(t) = \sum_n I^{(n)}(t) = \sum_n I_0^{(n)} \exp\left(-\frac{t}{\tau_f^{(n)}}\right), \quad (6)$$

where $I^{(n)}(t)$, $I_0^{(n)}$, and $\tau_f^{(n)}$ are the temporal fluorescence intensity, initial emission intensity, and lifetime of the nth type of the fluorophore, respectively.

For the parallel component [20]:

$$I_\parallel(t) = \sum_n I_\parallel^{(n)}(t) = \sum_n \frac{I_0^{(n)}}{3} \exp\left(-\frac{t}{\tau_f^{(n)}}\right)\left(1 + 2r_0^{(n)} \exp\left(-\frac{t}{\tau_r^{(n)}}\right)\right), \quad (7)$$

where $r_0^{(n)}$ is the initial anisotropy at $t = 0$ of the nth type of the fluorophore.

There are two types of molecules ($n = 2$) in our case: cell-bound and -unbound Cybesin (Cytate) molecules. It is reasonable to assume that they both have the same fluorescence lifetime [$\tau_f^{(1)} = \tau_f^{(2)}$]. The cell-bound contrast agents have infinite rotation time [$\tau_r^{(1)} \to \infty$] because they are bound with a huge tissue cell, and their rotations are too slow in comparison with the rotational time [$\tau_r^{(2)}$] of the unbound Cybesin (Cytate), which is in the range of picoseconds. It is also reported that fluorescence intensity is proportional to the number of fluorophores [21]. By taking these assumptions, $I_\parallel(t)$ can be written as the following equation:

$$I_\parallel(t) = \frac{I_0}{3} \exp\left(-\frac{t}{\tau_f}\right)\left(1 + 2r_1 + 2r_0 \exp\left(-\frac{t}{\tau_r}\right)\right), \quad (8)$$

where r_1 stands for the static anisotropy of cell-bound Cybesin (Cytate) molecules in prostate tissue.

Using similar procedure of derivation, the perpendicular component can be obtained as:

$$I_\perp(t) = \frac{I_0}{3} \exp\left(-\frac{t}{\tau_f}\right)\left(1 - r_1 - r_0 \exp\left(-\frac{t}{\tau_r}\right)\right). \quad (9)$$

Substituting Eqs. (8) and (9) into Eq. (1), the time-dependent fluorescence anisotropy of contrast agents becomes:

$$r(t) = r_1 + r_0 \exp\left(-\frac{t}{\tau_r}\right). \quad (10)$$

The temporal profiles of the fluorescence anisotropy $r(t)$ depends only on r_1 (the static anisotropy of fluorophores), r_0 (the initial temporal anisotropy at $t = 0$ of the fluorophores), and τ_r (the dipole's rotation time) but not on τ_f (the fluorophore's lifetime).

Introducing Eqs. (8) and (9) into $I(t) = I_\parallel(t) + 2I_\perp(t)$, the total time-resolved fluorescence intensity can be obtained the same as in Eq. (5).

4. Experimental Results and Discussion on Time-Resolved Measurements

Six Cybesin (Cytate)-stained cancerous and six Cybesin (Cytate)-stained normal prostate tissue samples were used for the time-resolved fluorescence measurements, respectively. The time-resolved fluorescence intensity profiles of $I_\parallel(t)$ and $I_\perp(t)$ averaged over six (6) samples for the cancerous and normal prostate tissues stained with Cybesin are displayed in Figs. 2(a) and 2(b), respectively. The thin-dashed and thin-dotted-curve profiles display the parallel and perpendicular components, respectively. The salient feature of Figs. 2(a) and 2(b) is that $I_\parallel$ is greater than $I_\perp$ throughout the decay period for both cancerous and normal tissues. At the peak position, $I_\parallel(0)$ is ~1.57 times stronger than $I_\perp(0)$ for cancerous tissue, while this ratio is ~1.40 for normal tissue. The solid lines display the fitting curves calculated using

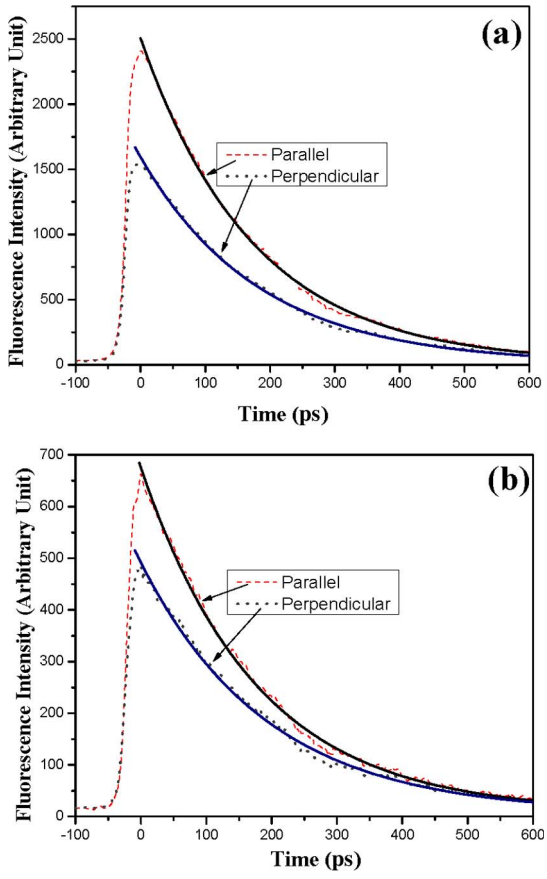

Fig. 2. (Color online) The time-resolved fluorescence intensity of light emitted from Cybesin-stained (a) cancerous and (b) normal prostate tissues with linearly polarized 800 nm laser excitation. The dashed- and dotted-curve profiles display the parallel and perpendicular components emitted from stained tissue, respectively. The solid lines display the fitting curves calculated using Eq. (8) for the parallel component and Eq. (9) for the perpendicular component, respectively.

Eq. (8) for the parallel component, and Eq. (9) for the perpendicular component, respectively.

The total time-resolved fluorescence intensities $I(t)$ and the temporal profiles of the fluorescence anisotropy $r(t)$ of Cybesin in stained prostate tissue were calculated using the data of $I_{\parallel}(t)$ and $I_{\perp}(t)$ shown in Fig. 2 and Eqs. (5) and (10), respectively. The calculated results of $I(t)$ and $r(t)$ are displayed in Figs. 3(a) and 3(b), respectively. Figure 3(a) indicates that the emission intensity from the Cybesin-stained cancerous tissue is higher than that from the Cybesin-stained normal tissue throughout the lifetime of the Cybesin emission. The emission peak intensity of the Cybesin-stained cancerous tissue is much greater than that of the Cybesin-stained normal tissue. The ratio of peak fluorescence intensities of Cybesin-stained cancerous tissue to normal prostate tissues is found to be $\sim 3.29 \pm 0.51$, indicating that the cancerous prostate tissue takes up more Cybesin than the normal tissue [7,8,10]. The interesting features of $r(t)$ curves shown in Fig. 3(b) are (i) the values of fluorescence anisotropy of Cybesin in the stained cancerous tissue are always larger than those of the stained normal tissue at all the decay times and (ii) the profile of $r(t)$ for the Cybesin-stained cancerous tissue shows a little flatter decay in comparison with the normal tissue.

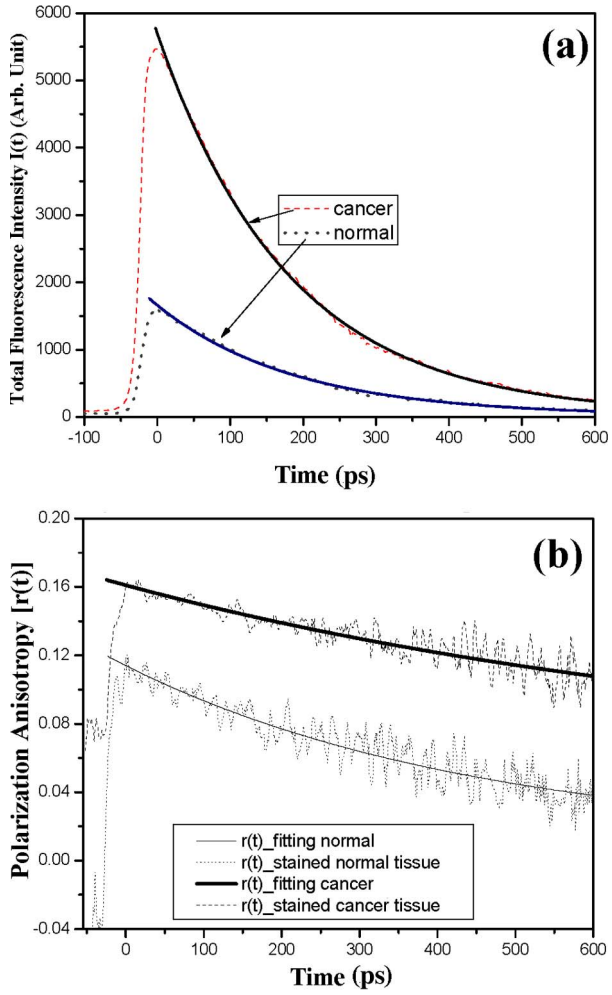

Fig. 3. (Color online) (a) The total emission intensity of Cybesin-stained cancerous (dashed curve) and normal (dotted curve) prostate tissues obtained using the data shown in Figs. 2(a) and 2(b), and Eq. (5) in the text. The solid lines display the fitting curves calculated using Eq. (5). (b) Time-dependent fluorescence anisotropy calculated using Eq. (1) in the text and the measured data shown in Figs. 2(a) and 2(b). The dashed and dashed–dotted curve profiles indicate the $r(t)$ for the stained cancerous and normal prostate tissues, respectively. The fitting curves for Cybesin in the cancer tissue (thick solid curve) and Cybesin in the normal tissue (thin solid curve) were calculated using Eq. (10) in the text and the corresponding data shown by the dashed and dashed–dotted curves in (b).

The random rotation of Cybesin (Cytate) molecules contributed to fluorescence will result in the decay behavior of $r(t)$. By investigating the time-resolved fluorescence and anisotropy of emission form Cybesin (Cytate) in prostate tissue, the biophysical microenvironments of contrast agents can be studied. The difference of the time-resolved total fluorescence intensity $I(t)$ shown in Fig. 3(a), and temporal anisotropies $r(t)$ for cancerous and normal prostate tissues shown in Fig. 3(b) can be quantified by fitting these experimental data using our analytic model. The fluorescence lifetime (τ_f) and initial peak intensity (I_0) of Cybesin in the stained cancerous and normal prostate tissues can be obtained by fitting the temporal profiles of the total emission shown in Fig. 3(a) using Eq. (5). Eqs. (8)–(10), and the temporal profiles of the polarized fluorescence and anisotropy data shown in Figs. 2 and 3(b) are used to obtain the parameters for Cybesin in stained cancerous and normal prostate tissues: τ_r (the rotation time), r_1 (anisotropy of the static component), and r_0 (the value of dynamical anisotropy for the rotation dipoles at $t = 0$). The fitting results are shown in Figs. 2 and 3 as solid curves for the cancerous and normal prostate tissues. The good agreement of our model fitting with the experimental data indicates that the time-resolved polarization-dependent fluorescence of the contrast agent (Cybesin) in human prostate tissue can be truly considered to have two contributions from the free Cybesin molecules remaining in the liquid of tissue and the static cell-bound Cybesin. The ratio of peak intensities of total fluorescence for Cybesin-stained cancerous tissue and normal tissues ($I_0^{\text{cancer}}/I_0^{\text{normal}}$) is $\sim 3.43 \pm 0.54$ [7,8,10]. The rotation time τ_r and static fluorescence anisotropy r_1 for Cybesin in cancerous tissue were found to be 1.4 times and ~10 times larger than those for normal prostate tissue, respectively.

The time-resolved polarization fluorescence profiles of Cytate in prostate tissue have similar features as Cybesin. The parameters of τ_f, τ_r, r_1, and r_0 for Cytate were analyzed and obtained using similar procedure as described above. The fitting results show that the ratio of $I_0^{\text{cancer}}/I_0^{\text{normal}}$ for Cytate-stained cancerous and normal prostate tissues is $\sim 3.47 \pm 0.57$, indicating that cancerous prostate tissue preferential uptakes Cytate than normal tissue [7,9,11]. The rotation time τ_r and static fluorescence

anisotropy r_1 for Cytate in cancerous tissue were found to be 1.6 and ~5 times larger than those for normal prostate tissue, respectively. These properties can be explained by the preferential adsorbing of contrast agents in cancerous tissue and the different structure between cancerous and normal prostate tissues [7,9,11].

For convenience, all the experimental and calculated values of the parameters, r_0, r_1, τ_f, and τ_r for the two receptor-targeted contrast agents (Cybesin and Cytate) in the cancerous and normal prostate tissues are listed in Table 1.

The rotation time (τ_r) and the lifetime (τ_f) of both Cybesin and Cytate in prostate tissue are in the same time scale (a few hundred picoseconds), indicating that time-resolved fluorescence polarization spectroscopy can be used to investigate rotational dynamics [13–15]. The larger r_1 observed in Cybesin (Cytate)-stained cancerous tissue compared with that in normal tissue (as indicated in Table 1) can be understood because of more uptake of Cybesin (Cytate) in cancerous prostate tissue. Furthermore, because the wavelength of 800 nm used for pumping is close to the strong absorption peak of Cybesin (Cytate) and cancerous tissue takes up more Cybesin (Cytate) than the normal tissue [7–11], the stained cancerous tissue will absorb more photons than the stained normal tissue. The Cybesin (Cytate) contained in the deep layer of the stained cancerous tissue will have less opportunity to be excited by the laser than those in the normal tissue. The perpendicular fluorescence component emitted from the Cybesin (Cytate) contained in the stained tissue has a greater contribution by the photons undergoing a longer optical path. The light emitted from the stained normal tissue undergoes more distance and scattering than that emitted from the stained cancerous tissue; thus, the r_1 values of the stained cancerous tissue are much larger than those of the stained normal tissue.

The fitting results also show $\tau_r^{\text{cancer}} > \tau_r^{\text{normal}}$ for both Cybesin and Cytate. This can be understood because the larger decay time of free (unbound) Cybesin (Cytate) molecules in the cancerous prostate tissue indicates higher cell density and decreased interstitial spacing between cells in the cancerous tissue compared to the normal tissue, which agrees with the change of the tissue structure during the evolution of the malignant tumor [22]. The higher cell density in the cancerous prostate tissue [12,22] gives the molecules less "free" rotation space. In addition, the dye crowds more in the cancerous tissue due to the fact that more molecules are bound to cell surfaces through ligands for prostate cancerous tissue. Whether molecules rotate or not, rapid internal motions due to the flexible structure between contrast agent molecules and tissue cells are also responsible to the decay time of the anisotropy [13,14], which depends on the ligand strengths. In this point of view, $\tau_r^{\text{cancer}} > \tau_r^{\text{normal}}$ somehow reflects the stronger conjugation ligand strength and more cell-bound contrast agents in the cancerous prostate tissue than those in the normal prostate tissue. This may be the reason behind the larger decay time of Cybesin (Cytate) in the cancerous prostate tissue compared to Cybesin (Cytate) in the normal prostate tissue.

5. Fluorescence Polarization Imaging

The preferential uptakes of Cytate (Cybesin) in cancerous prostate tissue and the polarization preservation property of emission of Cytate (Cybesin) in prostate tissue can be used to enhance the imaging contrast between cancerous and normal tissue areas using fluorescence polarization difference imaging (FPDI) techniques [23]. In the imaging measurements, a small piece of cancerous prostate tissue and a small piece of normal prostate tissue stained with Cytate covered by a large piece of host normal prostate tissue with ~0.5 mm thickness were investigated. The polarized fluorescence images of this Cytate-stained cancerous/normal prostate tissue sample recorded with $\lambda_{\text{pump}} = 750$ nm and $\lambda_{\text{detection}} = 850$ nm are shown in Fig. 4. The parallel image shown in Fig. 4(a) was recorded when the polarization direction of detection was parallel (∥) to that of the illuminating beam. The perpendicular image shown in Fig. 4(b) was recorded when the polarization direction of detection was perpendicular (⊥) to that of the illuminating beam. Figure 4(c) displays the difference image obtained by subtracting the perpendicular image [Fig. 4(b)] from the parallel image [Fig. 4(a)]. Figures 4(d)–4(f) show the digital spatial cross-section intensity distributions of the stained tissue area in the images shown in Figs. 4(a)–4(c), respectively.

It can be seen from the images that the cancerous tissue area is much brighter than that of the normal tissue area. To quantify the difference, the intensity of the cancerous or normal tissue areas is calculated as $I_c = I_c^{\max} - I_{\text{background}}$ and $I_n = I_n^{\max} - I_{\text{background}}$, respectively, where $I_{\text{background}}$ is the background intensity, and $I_c^{\max}$ and $I_n^{\max}$ are the maximum intensities of the cancerous and normal tissue areas shown in Figs. 4(d)–4(f), respectively. The ratio of imaging intensities of cancerous to normal tissue areas is calculated using the equation of $r = 1_c/I_n$. Using the

Table 1. Comparison of Time-Resolved Emission Parameters of Cybesin and Cytate in Cancerous and Normal Prostate Tissues

Contrast Agent	r_1	r_0	τ_f (ps)	τ_r (ps)
Cybesin in cancer	0.056 ± 0.01	0.105 ± 0.01	179 ± 6.8	850 ± 150
Cybesin in normal	0.005 ± 0.01	0.103 ± 0.01	189 ± 11	600 ± 200
Cytate in cancer	0.062 ± 0.013	0.115 ± 0.012	118 ± 2.7	900 ± 180
Cytate in normal	0.014 ± 0.004	0.109 ± 0.030	123 ± 4.9	550 ± 140

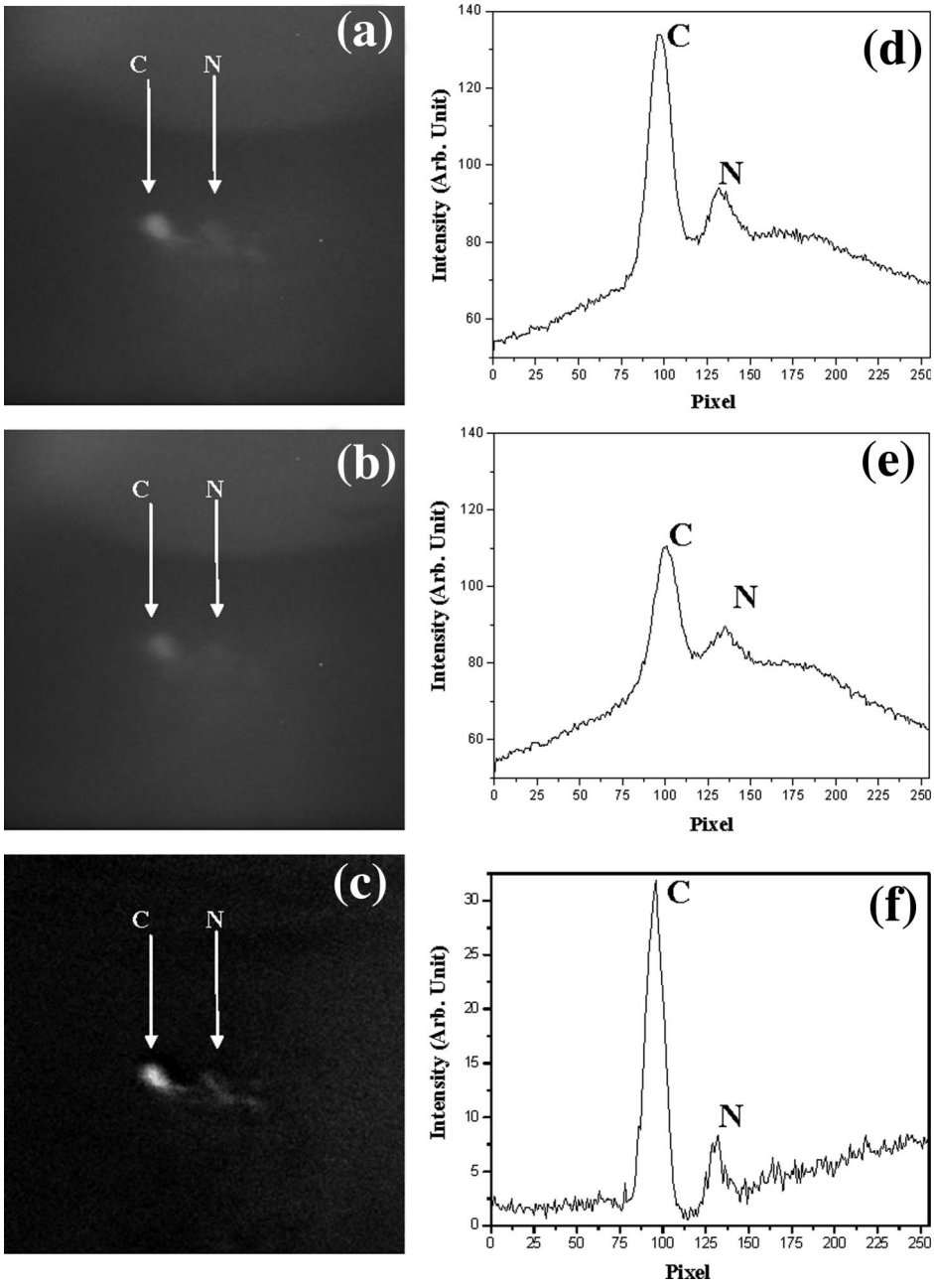

Fig. 4. Contrast agent fluorescence polarization images of a cancerous/normal prostate tissue sample consisting of a tiny Cytate-stained cancerous and a tiny Cytate-stained normal prostate tissue covered by large pieces of host normal prostate tissue. The images were recorded at $\lambda_{\text{pump}} = 750\,\text{nm}$ and $\lambda_{\text{detection}} = 850\,\text{nm}$ when the polarization direction in front of the CCD camera is (a) parallel and (b) perpendicular to that of the illuminating light. (c) Polarization difference image obtained by subtracting (b) from (a). (d)–(f) Digital spatial cross section intensity distributions of the images shown in (a)–(c) at a row crossing the areas of the stained cancerous (C) and normal (N) tissues, respectively.

digital data shown in Figs. 4(d) and 4(e), the ratio of imaging intensities of cancerous-to-normal areas is found to be ~3.69 for the parallel image and ~3.51 for the perpendicular image. These ratios are in good agreement with that obtained from the time-resolved fluorescence measurements.

The salient feature is that the relative contrast of the cancerous to the normal tissue areas in the polarization difference image shown in Fig. 4(c) is obviously higher than those in the individual polarization images shown in Figs. 4(a) and 4(b). Using the digital data shown in Fig. 4(f), the ratio of imaging intensities of cancerous to normal areas is found to be ~4.84 for the FPDI image. The contrasts (C) of the cancerous area to the normal area for all of the images shown in Fig. 4 were calculated using:

$$C = \frac{I_c - I_n}{I_c + I_n}, \tag{11}$$

where I_c and I_n are the local maximum intensities of the stained cancerous and normal tissue areas, respectively. Using the digital data shown in Figs. 4(d)–4(f), the contrasts for these parallel, perpendicular, and polarization difference images are calculated to be 0.57, 0.54, and 0.67, respectively.

In addition, the improvement of the spatial resolution of the difference image in comparison with the individual polarization images can be seen from Figs. 4(d)–4(f). The full-width at half-maximum (FWHM) for the cancerous tissue area shown in Fig. 4(f) is improved by a factor of 1.9 with respect to that of the individual parallel or perpendicular image. The improvement of the spatial resolution of the difference image can be understood because the fluorescence polarization difference image canceled out the strong diffusive component and only kept ballistic photons and partial snake photons from the fluorescent objects [24]. Because the difference of $I_{\parallel} - I_{\perp}$ for the Cytate-stained cancerous tissue is larger than that in the Cytate-stained normal tissue, the contrast between cancerous and normal tissue areas is improved.

Control experiments between a nonspecific contrast agent, ICG, and a specific contrast agent, Cybesin, were performed as well. NIR spectral polarization imaging experiments were used to demonstrate if the increased fluorescence seen in cancerous tissue is truly from the specific targeting of the corresponding receptor. The experimental results indicate that ICG-stained prostate cancerous and normal tissues show trivial difference in the fluorescence emission images. In addition, Achilefu *et al.* at Washington University reported that ICG does not bind to, leak to, nor localize in bombesin- and somatostatin-receptor-rich tumor tissues in animal models *in vivo* [7].

Prostate cancer is classified as an adenocarcinoma, or glandular cancer, which is developed from epithelial cells [25]. Of prostate cancer cases, 70% arise in the peripheral zone. Our methods are concentrated on layers of cells near the surface, so that a time of ~10 min for soaking samples in Cybesin (Cytate) solution was used [25]. Because of the mean mucosa thickness of $830 \pm 60\,\mu$m and the mean rectal wall thickness of 2.57 ± 0.15 mm [26,27], the NIR pumping light of 750 to 800 nm can penetrate the rectal wall to reach the prostate for optical imaging if irradiating from the rectum [10,27]. Previous spectral polarized imaging experiments performed at the Institute for Ultrafast Spectroscopy and Lasers show that an ICG-stained small object hidden inside the host prostate tissues in the rectum membrane/prostate structures at depths of 7.5 mm can be imaged and identified using fluorescence imaging methods [27]. ICG is the fluorescent part of Cybesin and Cytate. It is reasonable to assume that this method may deal with target depths at several millimeters under optimal conditions.

6. Conclusion

In summary, an analytical model to describe the emission behavior of the receptor-targeted contrast agents, Cybesin and Cytate, in prostate tissue was developed. A static fluorescence anisotropy component formed by the emission of prostate tissue cell-bound Cybesin (Cytate) molecules (with very slow rotation), and a time-dependent fluorescence anisotropy component formed by the emission of unbound Cybesin (Cytate) molecules (with fast rotation) were determined. This model was successfully used to explain the experimental results for Cybesin (Cytate) in stained cancerous and normal prostate tissues. The static fluorescence anisotropy value of Cybesin (Cytate) in the stained cancerous tissue was found to be much larger than that in the stained normal tissue, indicating more uptake of Cybesin (Cytate) in the cancerous prostate tissue. The larger rotation time of Cybesin (Cytate) in the cancerous tissue suggests higher cell density in cancerous tissue compared with the normal tissue. A stronger intensity of emission from the Cytate-stained cancerous prostate tissue in comparison with the stained normal tissue was also observed in the fluorescence polarization imaging measurements, indicating preferential uptakes of Cytate in the cancerous prostate tissue.

7. Future Work

In order to analyze the time-resolved signals from overlapped tumor and normal tissues, one first needs to investigate the picosecond emission spectrum of cancerous and normal tissue separately. Because cancerous tissue is usually surrounded by normal tissue, methods need to be developed to handle the mixing signal from both cancerous and normal prostate tissues to serve the purpose of clinical application in the future. The methods introduced in this study are designed to separately obtain the characteristic feature and profile of each time-resolved emission spectrum of the cancerous or normal prostate tissue but not to handle the double-layer tissue, in which measurements include signals from both the tumor and normal tissues. This study would provide an important basis to decompose the signals from the tumor and normal tissues. In future research, we are planning to use blind source separation methods: such as nonnegative matrix factorization, and multivariate curve resolution with alternating least-squares [28] to analyze the mixing time-resolved signals from tumor and normal tissues, and extract their individual contributions to the measured spectra.

Several biomedical studies are also needed to follow this spectral and optical imaging investigation. Some immunochemical analysis is needed to identify the bombesin (somatostatin) receptor subtype that is targeted by Cybesin (Cytate). The histological experiments for validating the difference of the bombesin (somatostatin) receptors between cancerous and normal prostate tissues are needed to be performed by collaborating with biology experts. Some work is also needed to study if rotational dynamics and

fluorescence anisotropies can be detectable in situations for the contrast agents inside and outside cells, because in viable cells, such as an *in vivo* situation, receptor-targeted probes can be internalized by tumor cells. We are planning to investigate this phenomenon in cultured prostate cancer cell lines of the scattering media and try to figure out a way to subtract the multiple scattering background in future research.

Appendix A: Derivation for Simplifying EQ. (A1) to EQ. (A2)

For the parallel component [20]:

$$I_{\parallel}(t) = \sum_{n} I_{\parallel}^{(n)}(t) = \sum_{\mathrm{n}} \frac{I_0^{(n)}}{3} \exp\left(-\frac{t}{\tau_f^{(n)}}\right)\left(1 + 2r_0^{(n)} \exp\left(-\frac{t}{\tau_r^{(n)}}\right)\right). \tag{A1}$$

There are two types of molecules ($n = 2$) in our case: cell-bound and unbound Cybesin (Cytate) molecules. They both have the same fluorescence lifetime [$\tau_f^{(1)} = \tau_f^{(2)}$]. The cell-bound contrast agents have infinite rotation time [$\tau_r^{(1)} \to \infty$] because they are bound with huge tissue cells, and their rotations are too slow in comparison with the rotational time [$\tau_r^{(2)}$] of unbound Cybesin (Cytate), which is in the range of picoseconds. Then $I_{\parallel}(t)$ can be written as the following equation:

$$\begin{aligned} I_{\parallel}(t) &= \sum_{2} I_{\parallel}^{(2)}(t) \\ &= \frac{I_0^{(1)}}{3} \exp\left(-\frac{t}{\tau_f^{(1)}}\right)\left(1 + 2r_0^{(1)} \exp\left(-\frac{t}{\tau_r^{(1)}}\right)\right) \\ &\quad + \frac{I_0^{(2)}}{3} \exp\left(-\frac{t}{\tau_f^{(2)}}\right)\left(1 + 2r_0^{(2)} \exp\left(-\frac{t}{\tau_r^{(2)}}\right)\right) \\ &= \exp\left(-\frac{t}{\tau_f}\right)\left(\frac{I_0^{(1)}}{3} + \frac{I_0^{(2)}}{3} + \frac{I_0^{(1)}}{3} 2r_0^{(1)} \right. \\ &\quad \left. + \frac{I_0^{(2)}}{3} 2r_0^{(2)} \exp\left(-\frac{t}{\tau_r^{(2)}}\right)\right). \end{aligned}$$

Because fluorescence intensity is proportional to the number of fluorophores in the tissue and the intensity of emission from a single Cybesin (Cytate) molecule [21], it is reasonable to assume $I_0^{(1)} = C \cdot I_0^{(2)}$, where C is the proportional coefficient describing the linear relationship between $I_0^{(1)}$ and $I_0^{(2)}$. Substituting $I_0^{(1)} = C \cdot I_0^{(2)}$ into $I_0 = I_0^{(1)} + I_0^{(2)}$, the total initial intensity can be written as $I_0 = (C + 1) \cdot I_0^{(2)}$. Therefore, $I_{\parallel}(t)$ can be written as:

$$\begin{aligned} I_{\parallel}(t) &= \exp\left(-\frac{t}{\tau_f}\right)\left(\frac{CI_0^{(2)}}{3} + \frac{I_0^{(2)}}{3} + \frac{I_0^{(2)}}{3} C2r_0^{(1)} \right. \\ &\quad \left. + \frac{I_0^{(2)}}{3} 2r_0^{(2)} \exp\left(-\frac{t}{\tau_r^{(2)}}\right)\right) \\ &= \frac{I_0^{(2)}}{3} \exp\left(-\frac{t}{\tau_f}\right)\left((C+1) + 2nr_0^{(1)} \right. \\ &\quad \left. + 2r_0^{(2)} \exp\left(-\frac{t}{\tau_r^{(2)}}\right)\right) \\ &= \frac{I_0^{(2)}(Cn+1)}{3} \exp\left(-\frac{t}{\tau_f}\right)\left(1 + 2\frac{C}{C+1} r_0^{(1)} \right. \\ &\quad \left. + 2\frac{1}{C+1} r_0^{(2)} \exp\left(-\frac{t}{\tau_r^{(2)}}\right)\right). \end{aligned}$$

By defining $r_1 = Cr_0^{(1)}/(C+1)$, $r_0 = r_0^{(2)}/(C+1)$, $\tau_r = \tau_r^{(2)}$ [because $\tau_r^{(1)} = \infty$, there is only one rotation time, $\tau_r^{(2)}$, that needs to be investigated], the time-resolved parallel fluorescence component, $I_{\parallel}(t)$ of the contrast agents in tissue can be modeled as:

$$I_{\parallel}(t) = \frac{I_0}{3} \exp\left(-\frac{t}{\tau_f}\right)\left(1 + 2r_1 + 2r_0 \exp\left(-\frac{t}{\tau_r}\right)\right). \tag{A2}$$

The expression of $I_{\parallel}(t)$ as the derived Eq. (A2) is the same as Eq. (8) in the text.

This research is supported by the U.S. Army Medical Research and Material Command by grant W81XWH-08-1-0717 (CUNY RF 47170-00-01). The authors acknowledge the help of the NDRI and the CHTN for providing normal and cancer prostate tissue samples for the measurements.

References

1. A. Jemal, R. Siegel, E. Ward, Y. Hao, J. Xu, and M. Thun, "Cancer statistics, 2009," CA Cancer J. Clin. **59**, 225–247 (2009).
2. R. R. Alfano, D. Tata, J. Cordero, P. Tomashefsky, F. Lonyo, and M. Alfano, "Laser induced fluorescence spectroscopy from native cancerous and normal tissue," IEEE J. Quantum Electron. **20**, 1507–1511 (1984).
3. D. B. Tata, M. Foresti, J. Cordero, P. Tomashefsky, M. A. Alfano, and R. R. Alfano, "Fluorescence polarization spectroscopy and time-resolved fluorescence kinetics of native cancerous and normal rat kidney tissues," Biophys. J. **50**, 463–469 (1986).
4. Y. Pu, W. B. Wang, B. B. Das, and R. R. Alfano, "Differences of time-resolved near infrared spectral wing emission and imaging of human cancerous and normal prostate tissues," Opt. Commun. **282**, 4308–4314 (2009).
5. K. C. Smith, *The Science of Photobiology*, 2nd ed. (Plenum, 1989).

6. D. J. Dean and B. J. Korte, "A new federal institute focuses on biomedical imaging and bioengineering," Opt. Photon. News **14**(10), 38–42 (2003).
7. J. E. Bugaj, S. Achilefu, R. B. Dorshow, and R. Rajagopalan, "Novel fluorescent contrast agents for optical imaging of *in vivo* tumor based on a receptor-targeted dye-peptide conjugate platform," J. Biomed. Opt. **6**, 122–133 (2001).
8. J. C. Reubi, S. Wenger, J. Schmuckli-Maurer, J.-C. Schaer, and M. Gugger, "Bombesin receptor subtypes in human cancers: detection with the universal radioligand $^{125}I - [D - \mathrm{TYR}^{6}, \beta - \mathrm{ALA}^{11}, \mathrm{PHE}^{13}, \mathrm{NLE}^{14}]$ bombesin(6-14)," Clin. Cancer Res. **8**, 1139–1146 (2002).
9. J. Hansson, A. Bjartell, V. Gadaleanu, N. Dizeyi, and P. A. Abrahamsson, "Expression of somatostatin receptor subtypes 2 and 4 in human benign prostatic hyperplasia and prostatic cancer," Prostate **53**, 50–59 (2002).
10. Y. Pu, W. B. Wang, G. C. Tang, F. Zeng, S. Achilefu, J. H. Vitenson, I. Sawczuk, S. Peters, J. M. Lombardo, and R. R. Alfano, "Spectral polarization imaging of human prostate cancer tissue using a near-infrared receptor-targeted contrast agent," Technol. Cancer Res. Treat. **4**, 429–436 (2005).
11. Y. Pu, W. B. Wang, B. B. Das, S. Achilefu, and R. R. Alfano, "Time-resolved fluorescence polarization dynamics and optical imaging of Cytate: a prostate cancer receptor-targeted contrast agent," Appl. Opt. **47**, 2281–2289 (2008).
12. D. F. Gleason and G. T. Mellinger, "Prediction of prognosis for prostate adenocarcinoma by combined histological and clinical," J. Urol. **111**, 58–64 (1974).
13. G. R. Fleming, J. M. Morris, and G. W. Robinson, "Direct observation of rotational diffusion by picosecond spectroscopy," Chem. Phys. **17**, 91–100 (1976).
14. G. Porter, P. J. Sadkowski, and C. J. Tredwell, "Picosecond rotational diffusion in kinetic and steady state fluorescence spectroscopy," Chem. Phys. Lett. **49**, 416–420 (1977).
15. R. D. Spencer and G. Weber, "Measurements of subnanosecond fluorescence life-times with a cross-correlation phase fluorometer," Ann. NY Acad. Sci. **158**, 361–375 (1969).
16. D. A. Beysens, G. Forgacs, and J. A. Glazier, "Cell sorting is analogous to phase ordering in fluids," Proc. Natl. Acad. Sci. USA **97**, 9467–9471 (2000).
17. J. P. Rieu and Y. Sawada, "Hydrodynamics and cell motion during the rounding of two dimensional hydra cell aggregates," Eur. Phys. J. B **27**, 167–172 (2002).
18. F. Pellegrino, P. Sekuler, and R. R. Alfano, "Picosecond fluorescence kinetics and polarization anisotropy from anthocyanin pigment," Photobiochem. Photobiophys. **2**, 15–20 (1981).
19. M. A. Dresner, P. J. Rossman, S. A. Kruse, and R. L. Ehman, "MR elastography of the prostate," ISMRM 99 CDs, http://cds.ismrm.org/ismrm-1999/PDF2/526.pdf.
20. R. Cubeddu, D. Comelli, C. D'Andrea, P. Taroni, and G. Valentini, "Time-resolved fluorescence imaging in biology and medicine," J. Phys. D: Appl. Phys. **35**, R61–R76 (2002).
21. S. A. Tatarkova, A. K. Verma, D. A. Berk, and C. J. Lloyd, "Quantitative fluorescence microscopy of macromolecules in gel and biological tissue," Phys. Med. Biol. **50**, 5759–5768 (2005).
22. A. Shmilovici, "Incomplete tumor volume reduction may improve cancer prognosis," Med. Hypoth. **68**, 1236–1239 (2007).
23. W. B. Wang, S. G. Demos, J. Ali, and R. R. Alfano, "Imaging fluorescence objects embedded inside animal tissue using a polarization difference technique," Opt. Commun. **142**, 161–166 (1997).
24. L. Wang, P. P. Ho, C. Liu, G. Zhang, and R. R. Alfano, "Ballistic 2-D imaging through scattering wall using an ultrafast Kerr gate," Science **253**, 769–771 (1991).
25. D. Theodorescu and T. L. Krupski, "Prostate cancer—biology, diagnosis, pathology, staging, and natural history," http://emedicine.medscape.com/article/458011-overview (2009).
26. C. H. Huh, M. S. Bhutani, E. B. Farfan, and W. E. Bolch, "Individual variations in mucosa and total wall thickness in the stomach and rectum assessed via endoscopic ultrasound," Physiol. Meas. **24**, N15–N22 (2003).
27. W. Wang, J. H. Ali, R. R. Alfano, J. H. Vitenson, and J. M. Lombardo, "Spectral polarization imaging of human rectum-membrane-prostate tissues," IEEE J. Sel. Top. Quantum Electron. **9**, 288–293 (2003).
28. Y. Pu, W. B. Wang, G. C. Tang, and R. R. Alfano, "Changes of collagen and NADH in human cancerous and normal prostate tissues studied using fluorescence spectroscopy with selective excitation wavelength," J. Biomed. Opt. **15**, 047008 (2010).